Progress In Electromagnetics Research B, Vol. 30, 337–353, 2011

RESONANCE WAVELENGTH DEPENDENCE AND MODE FORMATION IN GOLD NANOROD OPTICAL ANTENNAS WITH FINITE THICKNESS

T. Dattoma, M. Grande*, R. Marani, G. Morea, V. Marrocco, and A. D'Orazio

Dipartimento di Elettrotecnica ed Elettronica, Politecnico di Bari, Via Re David 200, Bari 70125, Italy

Abstract—In this paper we analyze the dependence of the resonance wavelength and mode formation of an optical gold nanorod antenna on its geometrical parameters in the wavelength range 500–1400 nm. In particular, we prove that nanoantennas differ from RF counterparts, since the minima and maxima, i.e., nodes and anti-nodes, of the resonant modes do not go to zero and show very intense peak at the corners due to non-negligible thickness. Moreover, FDTD simulations reveal that the usually considered linear relation between the resonant wavelength and the nanorod length has to be modified when the nanorod thickness is taken into account.

1. INTRODUCTION

Optical nanoantennas are metal nanostructure-based devices able to convert the energy coming from free propagating radiation into localized energy and vice versa [1–3]. These nanoscaled metallic structures possess a wide variety of extraordinary optical properties which assume essential roles in applications such as efficient light localization [4, 5], high resolution microscopy and spectroscopy [6–8], sensing [9, 10], photodetection [11, 12], light emission [13–15] and photovoltaics [16–18]. For many years technological difficulty in accessing nanoscale accuracy has strongly slowed down nanoantennas development, but in the last decade the impressive improvements in nanotechnology have removed this main limit and opened up the possibility to build antennas operating in the visible and infrared spectral ranges [19, 20].

Received 21 April 2011, Accepted 17 May 2011, Scheduled 22 May 2011

* Corresponding author: Marco Grande (grande@deemail.poliba.it).

The optical characteristics of differently shaped optical antennas (monopole antennas, dipole antennas, Yagi-Uda antennas, particle antennas, slot antennas, patch antennas, gap antennas) and the dependence of the antenna field enhancement and spectral response on the geometrical parameters have been already deeply discussed [21–35], also comparing both numerical [33] and experimental [32] results. Moreover, the scattering and absorption properties attributable to single noble metal nanoparticle having different shape (spherical, hemispherical, rectangular prism, triangular prism, cross-shape, etc...) and patterned nanoparticle arrays with different period have also been thoroughly investigated [36–39].

The design of an optical nanoantenna requires great attention since the conventional radiofrequency and microwave design rules that describe antenna parameters as a function of the operating wavelength are no longer valid [1–3]. In the high frequency regime, where the nanoantenna works, the metals show a strongly dispersive behaviour and their physical properties approach those of dielectrics. Therefore, since metals at optical frequencies behave in a different fashion with respect to perfect conductors, the electromagnetic field is not perfectly reflected by the metal surface and, on the contrary, penetrates inside the metal at a well-determined depth (skin depth). This relevant penetration depth is the consequence of the increased inertia, exhibited by the conductor electrons as an external optical radiation is applied, which determines a delay in their response. Moreover, as immediate effect of this phenomenon, at optical frequencies the incident radiation couples to the electron plasma, which models the metal electrons, causing the formation of rapid oscillations. The implicit consequence of this event is that electrons in metals do not respond to the wavelength of the incident radiation λ but to an effective wavelength λ_{eff} that can be expressed by a simple linear scaling rule as a function of the incident beam wavelength and of the plasma wavelength λ_p [40]. Other important challenges, not deeply explored yet, in the design of optical nanoantennas are: the impedance matching between the antenna and the source, the electro-optical transduction, the phase control of coupled optical antennas, antenna feeding, the dependence of the transmitting and receiving antenna on the radiation pattern, on the angular response pattern, on the type of antenna and on the characteristics of the surrounding medium and so on [41–46].

In this paper we will discuss, for the first time to the best of our knowledge, the dependence of resonant wavelengths of an optical nanoantenna, which is a gold nanorod located on a Gallium Nitride (GaN) substrate, on its geometrical parameters. We will show how resonant modes are generated and distributed on the metal-

dielectric interfaces. The electric field distributions, evaluated in the nanoantenna region through the spatial Discrete Fourier Transform (DFT), will be compared with those of the RF antenna counterparts. Finally, we will show how the geometrical parameters such as length and thickness affect the nanoantenna resonant wavelength.

2. DEFINITION OF THE NANOANTENNA GEOMETRY AND NUMERICAL METHOD

Figure 1 shows the sketch of the structure under investigation. It consists of a gold nanorod placed on a substrate of gallium nitride. The choice of gallium nitride as substrate is due to its optical properties, since this dielectric can be successfully employed as active material or in nonlinear nanoantennas-based applications.

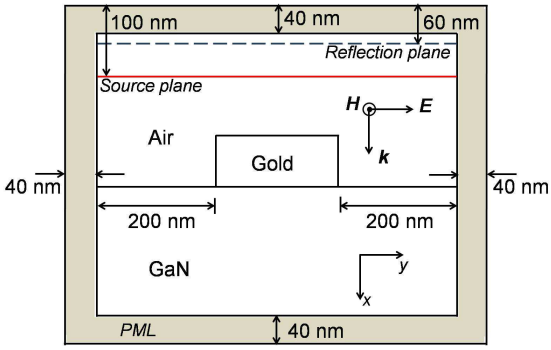

Figure 1. Sketch of the analyzed structure and definition of the computational domain.

The numerical analysis has been performed by using an open-source Finite Difference Time Domain (FDTD) code [47]. The implementation of metallic objects requires the definition of a model able to fit the experimental data of gold complex dielectric permittivity [48]. The following relation describes the Drude-Lorentz model [49] used to model Au physical properties:

$$\varepsilon_m(\omega) = \varepsilon_\infty - \frac{\omega_D^2}{\omega^2 + j\omega\gamma_D} - \sum_{k=1}^{2} \frac{\delta_k \omega_k^2}{\omega^2 - \omega_k^2 + 2j\omega\gamma_k} \tag{1}$$

where ε_∞ is the metal dielectric constant at the high frequency regime in the Drude model, ω_D and γ_D are the plasma and collision frequencies of the free electron gas related to the Drude model, whereas δ_i, ω_i and

γ_i, $i = 1, 2$, define amplitude, resonant angular frequency and damping constant of each Lorentz-like oscillator, respectively. The values of each parameter of the dielectric function model, fitting the experimental data of gold reported in [50] are: $\varepsilon_\infty = 5.398$, $\omega_D = 1.398 \cdot 10^{16}$ rad/s, $\gamma_D = 1.033 \cdot 10^{14}$ rad/s, $\delta_1 = 0.681$, $\omega_1 = 4.274 \cdot 10^{16}$ rad/s, $\gamma_1 = 4.353 \cdot 10^{14}$ rad/s, $\delta_2 = 1.861$, $\omega_2 = 5.225 \cdot 10^{16}$ rad/s and $\gamma_2 = 6608 \cdot 10^{14}$ rad/s [51].

Moreover, the considered geometrical parameters of the gold nanorod, length L and thickness d, range from 150 nm up to 850 nm and from 20 nm up to 200 nm, respectively. Without loss of generality and focusing on the main goal of the current study, the refractive index of the gallium nitride substrate [52], the ordinary one (n_o), has been fixed to the constant value of 2.36. Anyway to test the effectiveness of our results, we have verified that, in the wavelength range of interest (500–1400 nm), when the dispersion of the material is taken into account, the following considerations are still valid.

The incident field for FDTD computation is a p-polarized plane wave having a Gaussian temporal behaviour, tuned between 500 nm and 1400 nm. The electric field (E), whose unique component is along the y-direction, and the polarization (P) are defined parallel to the nanorod whilst the magnetic field comes out from figure plane (z-direction).

In all calculations, the excitation surface and the reflection plane are placed 100 and 60 nm, respectively, far from the top boundary. The spatial resolution is set equal to 2 nm in both the directions of the computational domain and 20 Perfectly Matched Layers (PMLs) are used to truncate the simulation area. The PML thickness is kept constant for each simulation and the distance between the nanorod and the domain boundaries is set equal to 200 nm on both sides in the y-direction.

3. ANALYSIS OF THE RESONANT MODE FORMATION

The first step of our analysis concerns the study of the resonance dependence on the nanoantenna geometry. Figure 2 shows the reflection spectra of a 20-nm-thick nanorod when the length is increased from 200 nm up to 700 nm. From the inspection of Figure 2 it is possible to argue that the resonances at higher wavelength are characterized by broader spectral profiles, whereas the resonances at lower wavelength are sharper. This specific behaviour of resonances implies increasingly weaker field localization as the relative wavelengths move to the upper limit of the considered spectral range. It is worth noting that this is valid for all resonant mode orders and structural

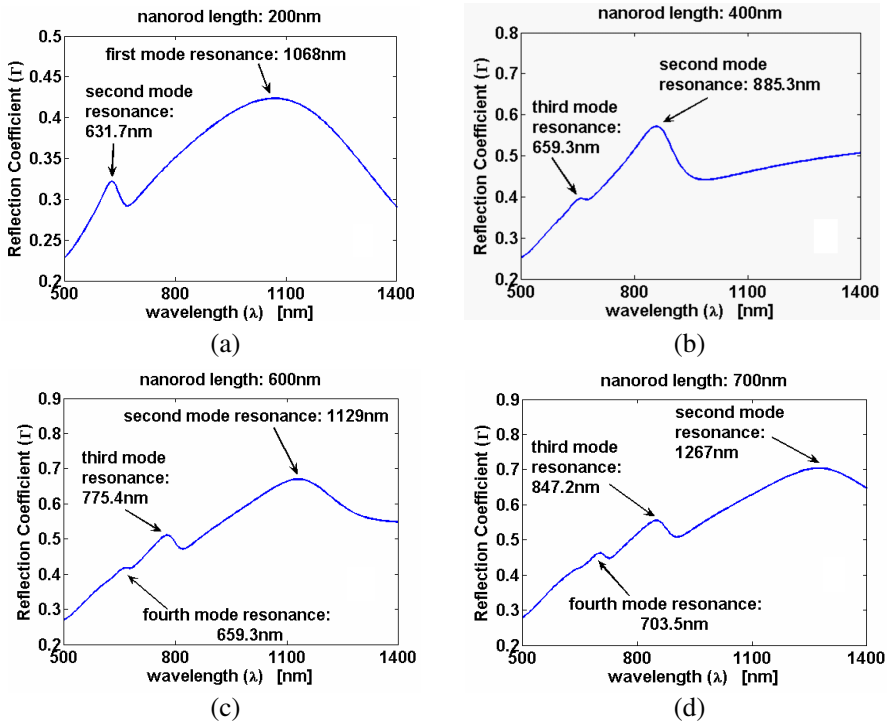

Figure 2. Reflection spectra of 20-nm-thick nanorods having length equal to (a) 200 nm, (b) 400 nm, (c) 600 nm and (d) 700 nm, respectively.

configurations [53, 54].

In addition, fixed the nanorod thickness, the resonant modes tend to move from lower to higher wavelengths as the nanorod length is increased changing their mode order. In Figure 2(a) (length $L = 200$ nm) the first order and the second order resonant modes are placed at wavelengths equal to $\lambda = 1068$ nm and $\lambda = 631$ nm, respectively. As the length increases (Figure 2(b) $L = 400$ nm, Figure 2(c) $L = 600$ nm, Figure 2(d) $L = 700$ nm), the first order mode pulls out of the spectral range of interest and the third order and the fourth order modes pull in. For instance, fixing the length $L = 400$ nm, the mode at the wavelength $\lambda = 885$ nm is a second order mode, while the mode at the wavelength $\lambda = 659$ nm is a third order mode.

Figure 3 shows the field distribution of different order modes evaluated for different lengths and resonant wavelengths of the nanoantenna: (a) first order mode ($L = 200$ nm and $\lambda = 1068$ nm), (b)

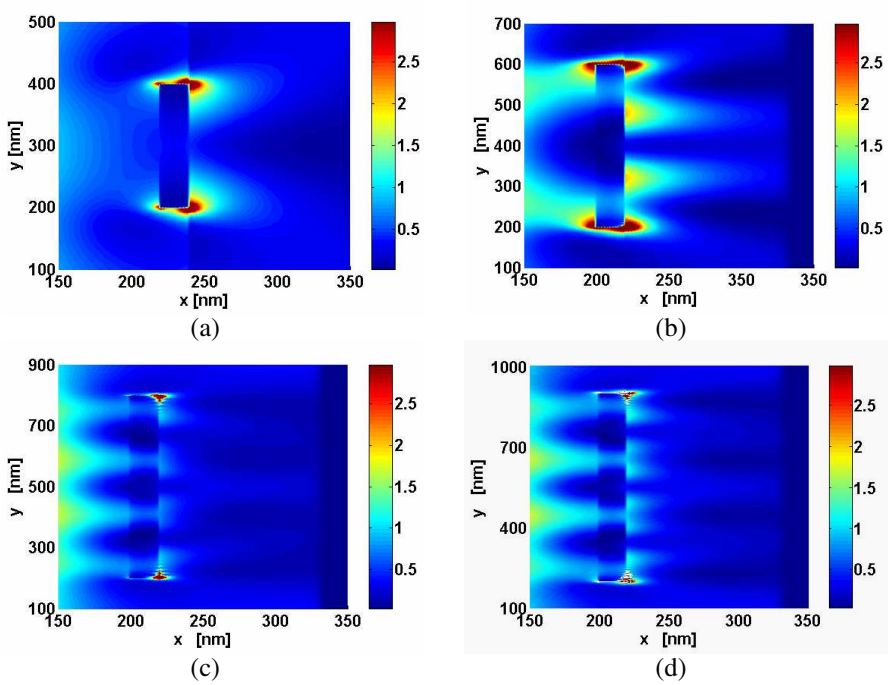

Figure 3. Details of the spatial Discrete Fourier Transforms of $|\bar{E}_{tot}|^2$ calculated at the resonant wavelength for the (a) first ($L = 200\,\text{nm}$ and $\lambda = 1068\,\text{nm}$), (b) second ($L = 400\,\text{nm}$ and $\lambda = 885\,\text{nm}$), (c) third ($L = 600\,\text{nm}$ and $\lambda = 659\,\text{nm}$) and (d) fourth ($L = 700\,\text{nm}$ and $\lambda = 703\,\text{nm}$) order modes reported in Figure 2 (d equal to 20 nm). The length of each nanoantenna has been chosen properly in order to show the first four orders of resonance.

second order mode ($L = 400\,\text{nm}$ and $\lambda = 885\,\text{nm}$), (c) third order mode ($L = 600\,\text{nm}$ and $\lambda = 659\,\text{nm}$) and (d) fourth order mode ($L = 700\,\text{nm}$ and $\lambda = 703\,\text{nm}$). This figure puts in evidence the effect of electric field localization at the metal-dielectric and metal-air interfaces. The field confinement at these interfaces is due to the greater value of the propagation constant with respect to the wave number in the dielectric, which determines the evanescently decay of field on both sides of each interface [55] and prevents it from propagating away from the interface. Therefore, along the interfaces Localized Surface Plasmon (LSP) can be individualized within the direction perpendicular to the nanorod surface, which is the oscillating direction of the conduction electrons. Moreover, at both interfaces the difference in the penetration depth [56]

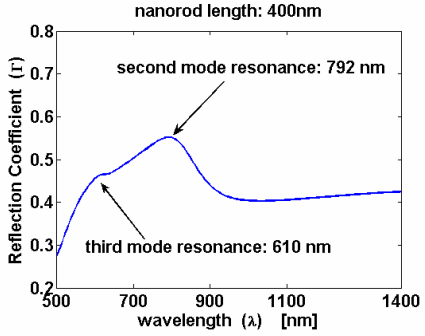

Figure 4. Reflection spectrum of 60-nm-thick nanorod having length L equal to 400 nm.

in the metal and dielectric layer can be emphasized, revealing a more consistent presence of field at the gold-GaN interface, since the refractive index of GaN is greater than that of the air.

Figure 4, which depicts the reflection spectrum when the antenna length and thickness are equal to 400 nm and 60 nm, respectively, allows to discuss also the dependence of the resonant wavelengths on the nanorod thickness. In particular, the comparison between the spectra reported in Figure 4 and Figure 2(b) highlights how, for a fixed length, resonant modes show tremendous difference in spectral positions as the nanorod thickness is varied. For instance the second mode resonance is placed at $\lambda = 885$ nm and $\lambda = 792$ nm for d equal to 20 nm and 60 nm, respectively. Therefore in the nanoantenna design we cannot prevent from taking into account the thickness as fundamental parameter.

In the optical plasmonic structure, for each resonant wavelength a LSP mode is excited with a field profile strongly affected by the choice of materials and elements shape [57]. Since the LSP resonance of the metal nanorod is able to direct light from the source emitter in a way resembling the radiowave and microwave antennas [25], whose field profiles along the metallic components are completely known, a comparison between the field of the analyzed nanoantenna and the field profiles of a RF dipole antenna becomes a straightforward topic. Hereinafter, we will consider only the Au/GaN interface because the resonances at the opposite face fall at lower wavelengths, where the gold absorption is not negligible and thus air-LSPRs do not interact with those emerging on the nanorod side which lies on GaN substrate.

Figure 5 shows the electric field profiles of each mode order, evaluated for nanoantennas having different lengths, as shown in the

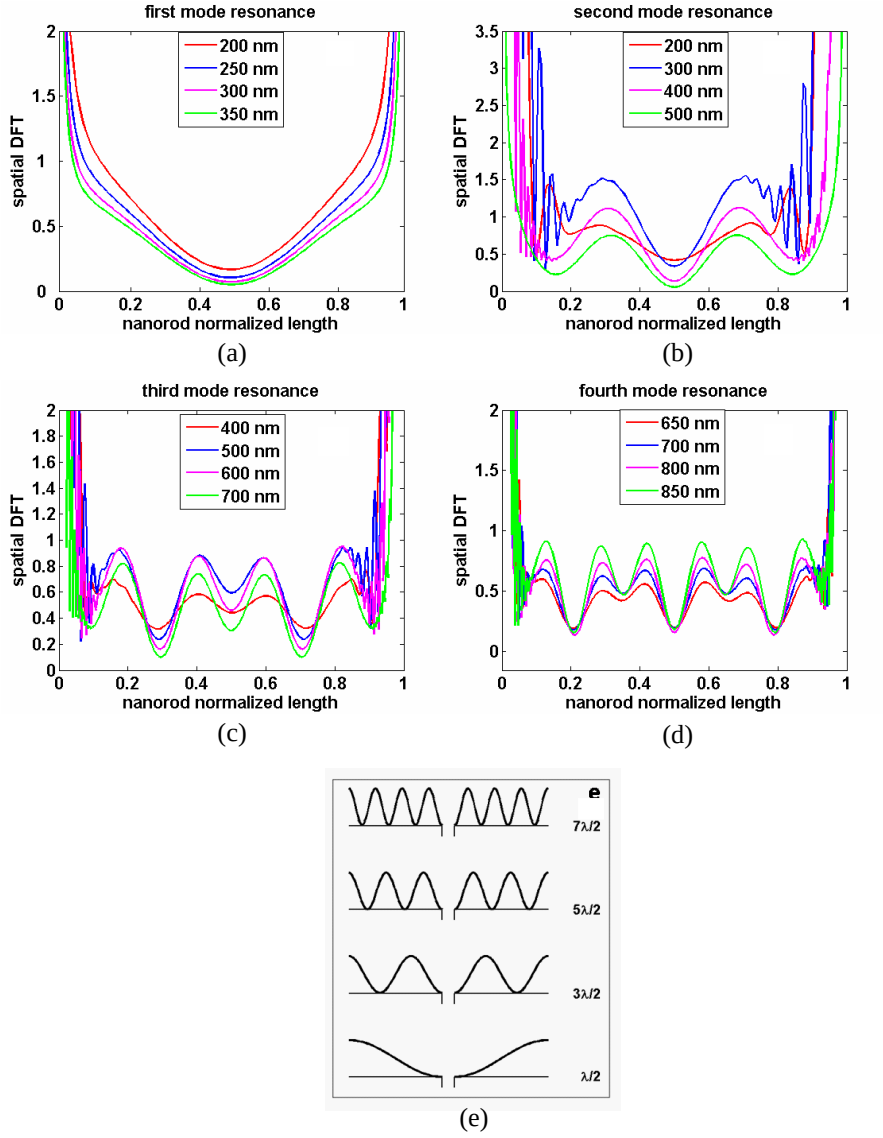

Figure 5. Distribution of the spatial $|\bar{E}_{tot}|^2$ DFT at the resonant wavelength for different lengths of the nanoantennas at Au/GaN interface; (e) field distribution $|\bar{E}_{tot}|^2$ of a RF dipole antenna reported here for comparison with nanoantenna dipole.

inset of the figure. To better visualize the graphs, the y-axis has been normalized to the longest one. As in the RF case, a full correspondence of the nodes and anti-nodes positions can be noted for all the considered lengths of the nanoantenna, but the profile minimum values do not reach the zero in the nanoantennas, due to the penetration of the field in the metal layer (skin effect). Furthermore, as the length increases, the difference among minima and maxima is accentuated showing the mode formation process and the diversity of the electric field profiles for each resonant mode.

Another important difference is related to the presence of high-localized spot at the nanoantenna corners due to the presence of the angled tips. Angled tips, together with the finite thickness, which is comparable to the nanoantennas length, induce the presence of highly intense spots, whose level is considerably huger than maxima peaks, as clearly observable in Figure 5. As a confirmation, when the thickness of the nanoantenna is reduced to the resolution step (2 nm) the peaks are still evident at the corners. In this way the mathematical solution of Maxwell's equations holds its validity, without being in contrast to the physical principle of scattering by corners. Instead, in the RF case, being the thickness negligible with respect to the electrical length, at the ends of the antenna, the entity of field is comparable with that in the maxima (Figure 5(e)).

In the RF dipole antenna, the resonance condition occurs when its length is equivalent to $n \cdot \lambda/2$ (n being an integer) and the resonance order can be easily individuated by observing the number of periods of the field wave along the metallic element. By analogy with the RF case, in the analyzed nanoantenna the resonance condition follows the equation [58]:

$$L = \left(m + \frac{1}{2}\right)\lambda_{\mathit{eff}} \quad (\text{with} \quad m = n - 1) \tag{2}$$

so that the first four resonance orders ($n = 1,\ 2,\ 3,\ 4$) correspond to nanoantenna lengths equal to $\lambda_{\mathit{eff}}/2,\ 3\lambda_{\mathit{eff}}/2,\ 5\lambda_{\mathit{eff}}/2,\ 7\lambda_{\mathit{eff}}/2$, respectively. Thus, for the first order the minimum of the distribution can be interpreted as the dipole-like configuration, while for the other three resonance orders two, four and six peaks are observable in the corresponding distribution respectively, as the graphs in Figure 5 reveal.

4. RESONANT WAVELENGTH RELATION

Fixed the nanorod thickness, for each mode order the effective resonant wavelength of each resonant mode depends linearly on the nanorod

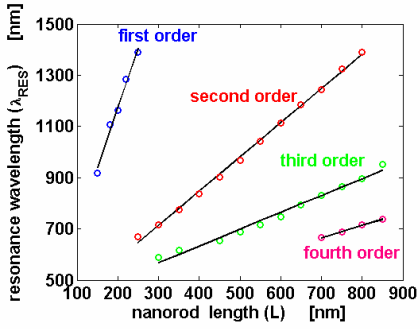

Figure 6. Resonant wavelength versus nanorod length of the first four resonant orders, to parity of the antenna thickness $d = 140\,\text{nm}$.

length [40], as we can see in Figure 6, where the thickness d of the nanorods has been fixed equal to 140 nm. However, as we have already outlined in the previous Paragraph, the nanorod thickness d strongly influences the mode formation and cannot be ignored in the analysis of a relation linking the resonant wavelength to the geometrical parameters of the nanorod. This dependence always rises even if the thickness of the nanorod is small enough to be considered negligible with respect to the operation wavelength, because of the excitation of LSP modes at Au/GaN interface whose field profiles, in the optical regime, do not vanish in the metal film. Therefore the linear relationship between the effective resonant wavelength and the nanorod length could be still expressed by the well known slope-intercept form, but without leaving out the thickness dependence [40]. Thus:

$$\lambda_{res}^{n}(d) = \alpha^{n}(d) \cdot L + \lambda_{0}^{n}(d) \tag{3}$$

where $\lambda_{res}^{n}(d)$ and n define the resonant wavelength and the n-th resonant order ($n = 1, 2, 3, 4$) and α^{n} and λ_{0}^{n} are the slope and the intercept with the y-axis, respectively. Once again, it is worth noting that all the parameters reported in Equation (3) are now expressed as a function of the nanorod thickness d.

With the intent of exploring how $\alpha^{n}(d)$ and $\lambda_{0}^{n}(d)$ vary with the thickness d for each resonant order mode, several nanoantennas, characterized by different values of thickness and length, have been extensively simulated and analyzed. In Figure 7 each circle depicts the evaluated slope $\alpha^{n}(d)$ and the intercept $\lambda_{0}^{n}(d)$, by changing the thickness d, for each resonant order mode. From the inspection of the figure, it is possible to claim that the slope and the intercept cannot be considered constant when the thickness is varied.

In order to describe the slope and intercept behavior with respect

to the thickness variation, three different fitting orders, namely constant (K), linear (L) and quadratic (Q), have been employed. The relative error is given by the following equation:

$$e = \sum_{d} \frac{\lambda_{\mathrm{FDTD}}(d) - \lambda_{res}(d)}{\lambda_{\mathrm{FDTD}}(d)} \tag{4}$$

where $\lambda_{\mathrm{FDTD}}(d)$ and $\lambda_{res}(d)$ are the resonant wavelength returned by the FDTD method and the linear relation reported in Equation (3), respectively. Table 1 summarizes the mean relative error estimated for each resonant order and fitting model when d spans between 20

Table 1. Relative errors obtained comparing resonant wavelength estimations with and without the thickness contribution.

	I mode (%)	II mode (%)	III mode (%)	IV mode (%)
K	7.4	4.9	9.6	3.1
L	5.6	1.8	2.9	2.8
Q	0.6	0.3	1.2	0.8

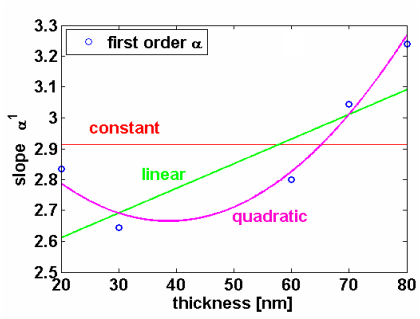

(a)

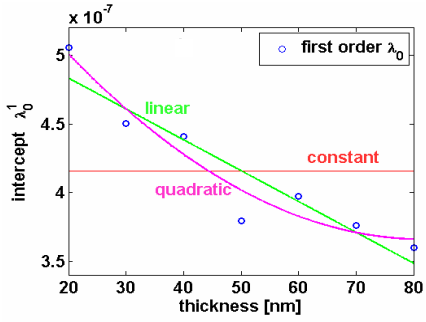

(b)

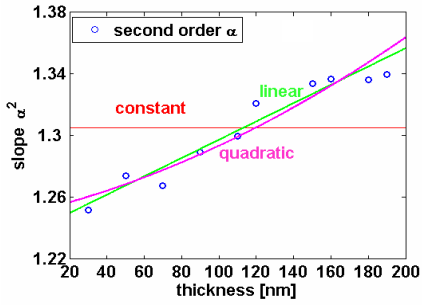

(c)

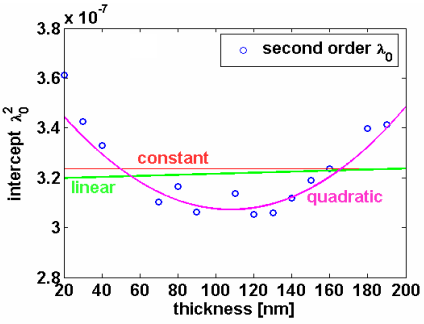

(d)

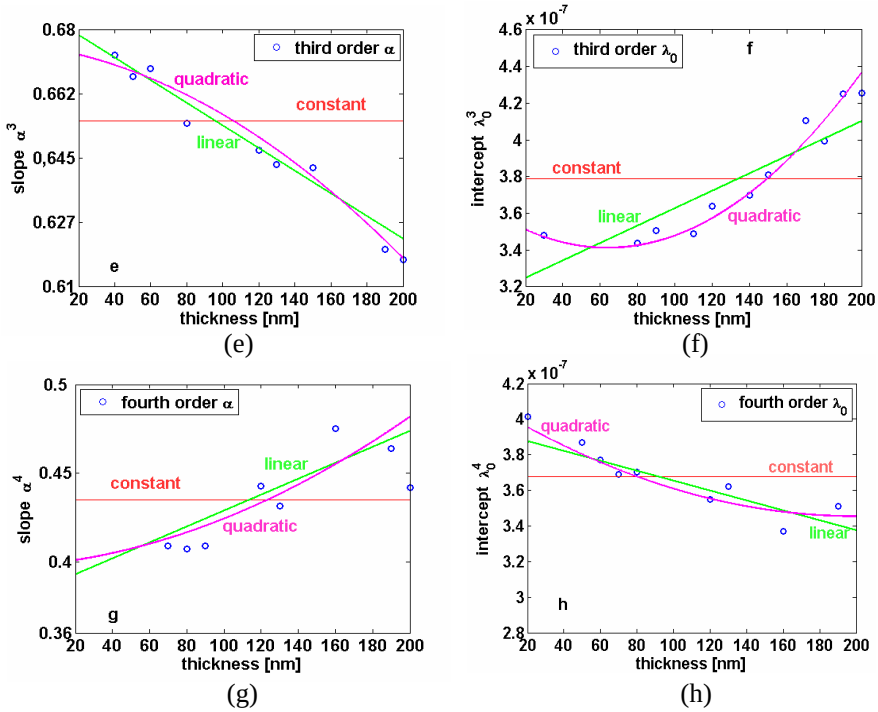

Figure 7. Slope $\alpha^n(d)$ and intercept $\lambda_0^n(d)$ for the (a)–(b) first, (c)–(d) second, (e)–(f) third and (g)–(h) fourth resonant mode.

and 200 nm. The inspection of Figure 7 and Table 1 reveals that the quadratic law optimally fits the coefficient of the linear relation of Equation (3). The relative error evaluated for the adopted quadratic relation is less than 1%, which is consistently smaller with respect to the constant case, where the dependence of the resonant wavelengths on the variation of the nanorod thickness is neglected.

As a consequence, a constant fit for the slope and intercept parameters leads to an absolute error of about 90 nm that corresponds to a huge error for a resonant optical elements such as nanoantennas. On the contrary the quadratic model, which takes into account the finite thickness of the nanorod, leads to relative error values always lower than about 9 nm.

5. CONCLUSIONS

In this paper we have discussed the complex relationship between the resonant mode formation and the geometry of optical nanoantennas

having finite thickness. In particular we have shown that, due to non-negligible thickness, gold nanorod antennas differ from RF counterparts since the minima and maxima (nodes and anti-nodes) do not go to zero and show very intense peaks at the corners. Nevertheless the mode profiles of the nanoantennas resemble the field distribution of the RF dipole antenna for all the analyzed resonant orders. Finally, the finite thickness of the nanorod in comparison with the length induces a change of the predicted resonant wavelength. The obtained results show how the dependence of the resonant wavelength on the nanoantenna thickness is strictly important for the design and the fabrication of the resonant elements to be used in optical systems for quantum and on-chip communication.

ACKNOWLEDGMENT

The authors would like to acknowledge COST action MP0702 on Towards Functional Sub-Wavelength Photonic Structures.

REFERENCES

1. Novotny, L. and N. van Hulst, "Antennas for light," *Nature Photonics*, Vol. 5, 83–90, 2011.
2. Bharadwaj, P., B. Deutsch, and L. Novotny, "Optical antennas," *Advances in Optics and Photonics*, Vol. 1, 438–483, 2009.
3. Park, Q.-H., "Optical antennas and plasmonics," *Contemporary Physics*, Vol. 50, No. 2, 407–423, 2009.
4. Devilez, A., B. Stout, and N. Bonod, "Mode-balancing far-field control of light localization in nanoantennas," *Phys. Rev. B*, Vol. 81, 245128, 2010.
5. Marrocco, V., M. A. Vincenti, M. Grande, G. Calò, V. Petruzzelli, F. Prudenzano, and A. D'Orazio, "Field localization in Bragg waveguide assisted by metal layers," *J. of Optical Society of America B*, Vol. 27, No. 4, 703–707, 2010.
6. Novotny, L. and S. J. Stranick, "Near-field optical microscopy and spectroscopy with pointed probes," *Ann. Rev. Phys. Chem.*, Vol. 57, 303–331, 2006.
7. Farahani, J. N., D. W. Pohl, H. J. Eisler, and B. Hecht, "Single quantum dot coupled to a scanning optical antenna: A tunable superemitter," *Phys. Rev. Lett.*, Vol. 95, No. 1, 017402, 2005.
8. Taminiau, T. H., R. J. Moerland, F. B. Segerink, L. Kuipers, and N. F. van Hulst, "$\lambda/4$ resonance of an optical monopole antenna

probed by single molecule fluorescence," *Nano Letters*, Vol. 7, No. 1, 28–33, 2007.

9. Kraziński, B. E., J. Radecki, and H. Radecka, "Surface plasmon resonance based biosensors for exploring the influence of alkaloids on aggregation of amyloid-β peptide," *Sensors*, Vol. 11, 4030–4042, 2011.
10. Anker, J. N., W. P. Hall, O. Lyandres, N. C. Shah, J. Zhao, and R. P. van Duyne, "Biosensing with plasmonic nanosensors," *Nature Materials*, Vol. 7, 442–453, 2008.
11. Cao, L., J. S. Park, P. Fan, B. Clemens, and M. L. Brongersma, "Resonant Germanium nanoantenna photodetectors," *Nano Letters*, Vol. 10, 1229–1233, 2010.
12. Wu, W., A. Bonakdar, and H. Mohseni, "Plasmonic enhanced quantum well infrared photodetector with high detectivity," *Applied Physics Letters*, Vol. 96, 161107, 2010. doi:10.1063/1.3419885.
13. Cubukcu, E., E. A. Kort, K. B. Crozier, and F. Capasso, "Plasmonic laser antenna," *Applied Physics Letters*, Vol. 89, 093120, 2006.
14. Dey, D., J. Kohoutek, R. M. Gelfand, A. Bonakdar, and H. Mohseni, "Composite nano-antenna integrated with quantum cascade laser," *IEEE Photonics Technology Letters*, Vol. 22, No. 21, 1580–1582, 2010.
15. Gao, H., K. Li, F. Kong, H. Xie, and J. Zhao, "Optimizing nano-optical antenna for the enhancement of spontaneous emission," *Progress In Electromagnetics Research*, Vol. 104, 313–331, 2010.
16. Pillai, S. and M. A. Green, "Plasmonics for photovoltaics applications," *Solar Energy Materials & Solar Cells*, Vol. 94, 1481–1486, 2010.
17. Marrocco, V., R. Marani, M. Grande, G. Morea, G. Calò, V. Petruzzelli, and A. D'Orazio, "Modification of the scattering of silver nanoparticles induced by Fabry-Pérot resonances rising from a finite Si layer," *Journal of Optics*, Vol. 13, 015004, 2011.
18. Marrocco, V., M. A. Vincenti, V. Petruzzelli, F. Prudenzano, and A. D'Orazio, "Efficient plasmonic nanostructures for thin film solar cells," *Photonics for Solar Energy Systems III*, *Proc. of SPIE*, Vol. 7725, 2010. ISBN 9780819481986, doi: 10.1117/12.862873.
19. Fumeaux, C., J. Alda, and G. D. Boreman, "Lithographic antennas at visible frequencies," *Optics Letters*, Vol. 24, No. 22, 1629–1631, 1999.

20. Simon, J. and F. J. Gonzales, "Nanoantennas for polarization division multiplexing," *Electronics Letters*, Vol. 47, No. 2, 120–121, 2011.
21. Taminiau, T. H., F. D. Stefani, F. B. Segerink, and N. F. van Hulst, "Optical antennas direct single-molecule emission," *Nature Photonics*, Vol. 2, 234–237, 2008.
22. Schuck, P. J., D. P. Fromm, A. Sundaramurthy, G. S. Kino, and W. E. Moerner, "Improving the mismatch between light and nanoscale objects with gold bowtie nanoantennas," *Phys. Rev. Lett.*, Vol. 94, 017402, 2005.
23. Alu, A. and N. Engheta, "Hertzian plasmonic nanodimer as an efficient optical nanoantenna," *Phys. Rev. B*, Vol. 78, 195111, 2008.
24. Bryant, G. W., F. J. G. de Abajo, and J. Aizpurua, "Mapping the plasmon resonances of metallic nanoantennas," *Nano Letters*, Vol. 8, 631–636, 2008.
25. Kosako, T., Y. Kadoya, and H. F. Hofmann, "Directional control of light by a nano-optical Yagi-Uda antenna," *Nature Photonics*, Vol. 4, 312–315, 2010.
26. Hofmann, H. F., T. Kosako, and Y. Kadoya, "Design parameters for a nanooptical Yagi-Uda antenna," *New J. Phys.*, Vol. 9, 217–217, 2007.
27. Li, J., A. Salandrino, and N. Engheta, "Shaping light beams in the nanometer scale: A Yagi-Uda nanoantenna in the optical domain," *Phys. Rev. B*, Vol. 76, 245403, 2007.
28. Kinkhabwala, A., Z. Yu, S. Fan, Y. Avlasevich, K. Müllen, and W. E. Moerner, "Large single-molecule fluorescence enhancements produced by a bowtie nanoantenna," *Nature Photon.*, Vol. 3, 654–657, 2009.
29. Guo, H., P. Meyrath, T. Zentgraf, N. Liu, L. Fu, H. Schweizer, and H. Giessen, "Optical resonances of bowtie slot antennas and their geometry and material dependence," *Optics Express*, Vol. 16, 7756–7766, 2008.
30. Kuehn, S., U. Hakanson, L. Rogobete, and V. Sandoghdar, "Enhancement of single-molecule fluorescence using a gold nanoparticle as an optical nanoantenna," *Phys. Rev. Lett.*, Vol. 97, 017402, 2006.
31. Bharadwaj, P. and L. Novotny, "Spectral dependence of single molecule fluorescence enhancement," *Opt. Express*, Vol. 15, 14266–14274, 2007.
32. González, F. J. and G. D. Boreman, "Comparison of dipole,

bowtie, spiral and log-periodic IR antennas," *Infrared Physics & Technology*, Vol. 46, No. 5, 418–428, 2005.

33. Fischer, H. and O. J. F. Martin, "Engineering the optical response of plasmonic nanoantennas," *Opt. Express*, Vol. 16, No. 12, 9144–9154, 2008.
34. Schuck, P., D. P. Fromm, A. Sundaramurthy, G. S. Kino, and W. E. Moerner, "Improving the mismatch between light and nanoscale objects with gold bowtie nanoantennas," *Phys. Rev. Lett.*, Vol. 94, 017402, 2005.
35. Biagioni, P., J. S. Huang, L. Du, M. Finazzi, and B. Hecht, "Cross resonant optical antenna," *Phys. Rev. Lett.*, Vol. 102, 256801, 2009.
36. Centeno, A., J. Breeze, B. Ahmed, H. Reehal, and N. Alford, "Scattering of light into silicon by spherical and hemispherical silver nanoparticles," *Optics Letters*, Vol. 35, No. 1, 75–78, 2010.
37. Centeno, A., F. Xie, and N. Alford, "Light absorption and field enhancement in two-dimensional arrays of closely spaced silver nanoparticles," *J. Opt. Soc. Am B*, Vol. 28, No. 2, 325–329, 2011.
38. Zhang, M., X. Zhou, and Y. Fu, "Plasmonic resonance excited extinction spectra of cross shaped Ag nanoparticles," *Plasmonics*, Vol. 5, 355–366, 2010.
39. Marrocco, V., M. A. Vincenti, A. Mongiello, M. De Sario, V. Petruzzelli, F. Prudenzano, and A. D'Orazio, "Gold nanorods in lineary modulated array," *Proc. of Metamaterials 2009, 3rd Int. Congr. On Advanced Electromagnetic Materials in Macrowaves and Optics*, London, 2009.
40. Novotny, L., "Effective wavelength scaling for optical antennas," *Phys. Rev. Lett.*, Vol. 98, 266802, 2007.
41. Alù, A. and N. Engheta, "Input impedance, nanocircuit loading, and radiation tuning of optical nanoantennas," *Phys. Rev. Lett.*, Vol. 101, 043901, 2008.
42. Locatelli, A., "Analysis of the optical properties of wire antennas with displaced terminals," *Opt. Express*, Vol. 18, No. 9, 9504–9510, 2010.
43. Ginzburg, P. and M. Orenstein, "Plasmonic transmission lines: From micro to nano scale with $\lambda/4$ impedance matching," *Opt. Express*, Vol. 15, 6762–6767, 2007.
44. Zhao, Y., N. Engheta, and A. Alù, "Effects of shape and loading of optical nanoantennas on its sensitivity and radiation properties," *Journal of Optical Society of America B*, 2011.
45. Balanis, C., *Antenna Theory: Analysis and Design*, John Wiley

and Sons, Inc., New York, NY, 1996.

46. Bean, J. A., B. A. Slovick, and G. D. Boreman, "Influence of substrate configuration on the angular response pattern of infrared antennas," *Opt. Express*, Vol. 18, No. 21, 21705–21713, 2010.
47. McMahon, J. M., JFDTD2D, http: www.thecomputationalphysici -st.com, 2009.
48. Veronis, G. and S. Fan, "Subwavelength plasmonic waveguide structures based on slots in thin metal films," *Proc. of SPIE*, Vol. 6123, 2006.
49. Stewart, M. E., N. H. Mack, V. Malyarchuk, J. A. N. T. Soares, T. W. Lee, S. K. Gray, R. G. Nuzzo, and J. A. Rogers, "Quantitative multispectral biosensing and 1D imaging using quasi-3D plasmonic crystals," *Proc. Nat. Acad. Sci.*, Vol. 103, 17143, USA, 2006.
50. Palik, E. D., *Handbook of Optical Constants of Solids*, Academic Press, San Diego, CA, 1998.
51. Pezzagna, S., J. Brault, M. de Micheli, P. Vennéguès, A. D. Wieck, and J. Massies, "GaN, a new material for integrated nonlinear optics," *Proc. of ECIO 2007*, Copenhagen, Denmark, Apr. 25–27, 2007.
52. McMahon, J. M., J. Henzie, T. W. Odom, G. C. Schatz, and S. K. Gray, "Tailoring the sensing capabilities of nanohole arrays in gold films with Rayleigh anomaly-surface plasmon polaritons," *Opt. Express*, Vol. 15, 18119, 2007.
53. Wang, F. and Y. R. Shen, "General properties of local plasmons in metal nanostructures," *Phys. Rev. Lett.*, Vol. 97, 206806, 2006.
54. Bozhevolnyi, S. I. and T. Sondergaard, "General properties of slow-plasmon resonant nanostructures: Nanoantennas and resonators," *Opt. Express*, Vol. 15, 10869, 2006.
55. Maier, S. A., *Plasmonics: Fundamentals and Applications*, Springer Science, New York, NY, 2007.
56. Barnes, W. L., A. Dereux, and T. Ebbesen, "Surface plasmon subwavelength," *Optics Nature*, Vol. 424, 824, 2003.
57. Boriskina, S. V. and L. Dal Negro, "Multiple-wavelength plasmonic," *Nanoantennas Opt. Lett.*, Vol. 35, 538, 2010.
58. Grenuche, P., S. Cherukulappurath, T. H. Taminiau, N. F. Van Hulst, and R. Quidant, "Spectroscopic mode mapping of resonant plasmon nanoantennas," *Phys. Rev. Lett.*, Vol. 101, 116805, 2008.